Ocean Sci. Discuss., 8, 2377–2415, 2011
www.ocean-sci-discuss.net/8/2377/2011/
doi:10.5194/osd-8-2377-2011

Ocean Science Discussions

Characteristics of the seasonal cycle of surface layer salinity in the global ocean

F. M. Bingham[1], **G. R. Foltz**[2], **and M. J. McPhaden**[3]

[1]Center for Marine Science, University of North Carolina Wilmington, 601 S. College Rd., Wilmington, NC 28403-5928, USA
[2]NOAA/Atlantic Oceanographic and Meteorological Laboratory, 4301 Rickenbacker Cswy, Miami, FL 33149, USA
[3]NOAA/Pacific Marine Environmental Laboratory, 7600 Sand Point Way NE, Seattle, WA 98115, USA

Received: 20 October 2011 – Accepted: 9 November 2011 – Published: 7 December 2011

Correspondence to: F. M. Bingham (binghamf@uncw.edu)

Published by Copernicus Publications on behalf of the European Geosciences Union.

Abstract

The seasonal variability of surface layer salinity (SLS), evaporation (E), precipitation (P) and $E - P$ over the global ocean is examined using in situ salinity data and the National Center for Environmental Prediction's Climate System Forecast Reanalysis. Seasonal amplitudes and phases are calculated using harmonic analysis and presented in all areas of the open ocean between 60° S and 60° N. Areas with large amplitude SLS seasonal variations include: the intertropical convergence zone in the Atlantic, Pacific and Indian Oceans; western marginal seas of the Pacific; and the Arabian Sea. The median value in areas that have statistically significant seasonal cycles of SLS is 0.19. Between about 60° S and 60° N, 37 % of the ocean surface has a significant seasonal cycle of SLS and 75 % a seasonal cycle of $E - P$. Phases of SLS have a bimodal distribution, with most areas of the ocean peaking in SLS in either March/April or September/October.

The same calculation is done with surface freshwater flux using a mixed-layer depth climatology. With the exception of an area near the western boundaries of the North Atlantic and North Pacific, seasonal variability is dominated by precipitation. Surface freshwater fluxes also have a bimodal distribution, with peaks in January and July, 1–2 months before the peaks of SLS.

The amplitudes and phases of SLS and surface fluxes compare well in a qualitative sense, suggesting that much of the variability in SLS is due to $E - P$ forcing. However, the amplitudes of SLS are somewhat larger than would be expected and the peak of SLS comes typically about one month earlier than expected. The differences of the amplitudes of the two quantities is largest in such areas as the Amazon River plume, the Arabian Sea, the ITCZ and the eastern equatorial Pacific and Atlantic, indicating that other processes such as ocean mixing and lateral transport must be important, especially in the tropics.

OSD

8, 2377–2415, 2011

1 Introduction

The salinity of the ocean surface layer (SLS) can be considered a proxy indicating the hydrologic cycle, or atmospheric transport of freshwater around the globe. Areas of relatively high SLS tend to be ones where evaporation is a dominant process with a net transport of freshwater from ocean to atmosphere. Conversely, areas of relatively low SLS tend to be ones where precipitation is a dominant process with a net transport of freshwater from the atmosphere to the ocean (Durack and Wijffels, 2010). The use of SLS in understanding the global hydrologic cycle is a major justification for two recent satellite missions to map sea surface salinity (SSS; the distinction between SSS and SLS will be discussed in the next section), NASA's Aquarius (Lagerloef et al., 2008) and ESA's SMOS (Berger et al., 2002).

The atmospheric part of the hydrologic cycle operates on a short time scale compared to the global ocean circulation. Typical residence time for water in the atmosphere is on the order of 7 days (Bengtsson, 2010), whereas ocean circulation processes can have time scales of years to decades. The hydrologic cycle is influenced by, and makes up a major part of, weather and climate on a local to global scale. Weather and climate, in turn, are driven by seasonally and latitudinally varying inputs of solar radiation. The most important time scale of variability in weather and climate is the seasonal, where intra-year changes in solar input cause changes in such features as the position of the intertropical convergence zone (ITCZ), paths of mid-latitude storm tracks, monsoon circulation particularly in the vicinity of east and south Asia, and changes in the temperature and humidity of the air that comes into close contact with the ocean. So in studying the interactions between ocean and atmosphere, we come across a mismatch of time scales, between a rapidly varying (days to months) atmosphere and a slowly varying (years to decades) ocean. The seasonal time scale sits right at the boundary between these scales, and thus makes an important contribution to the freshwater exchanges between atmosphere and ocean that control each one.

OSD
8, 2377–2415, 2011

While SLS varies on many different time and space scales (Tomczak, 1995), here we focus on the seasonal cycle – variability that is phase-locked to the calendar. The global seasonal cycle of SLS has been studied in the past by Boyer and Levitus (2002), who published maps of the amplitude and phase of the seasonal harmonic of SLS based on the 1998 World Ocean Atlas monthly gridded values (Boyer et al., 1998a,b,c). SLS at the seasonal time scale is certainly influenced by surface fluxes (Delcroix and Henin, 1991; Delcroix et al., 1996) and in some areas by other processes such as vertical mixing, entrainment and horizontal advection (Foltz et al., 2004; Foltz and McPhaden, 2008; Johnson et al., 2002). In the tropics, between 10° N and 5° S, the most dominant element of surface forcing at the seasonal scale is precipitation variability associated with meridional migration of the ITCZ (da Silva et al., 1994). Evaporation is the dominant process in winter near the western boundaries mainly associated with cold air outbreaks (Yu et al., 2008).

There have been many regional efforts to study the seasonal variability of SSS especially in the tropical oceans, including the Pacific (Delcroix and Henin, 1991; Bingham and Lukas, 1996; Delcroix et al., 1996, 2005; Gouriou and Delcroix, 2002), Atlantic (Dessier and Donguy, 1994; Foltz and McPhaden, 2008) and Indian (Rao and Sivakumar, 2003). Rao and Sivakumar for example show maps of annual average SSS, annual variance, maps for each month and amplitude and phase of the annual cycle. In the Arabian Sea and Bay of Bengal they show large seasonal amplitudes of up to 0.7 and quite large variability in the phase. Ren and Riser (2009) studied the seasonal balance of mixed-layer salinity in a region of the northeastern subarctic Pacific. They found the mixed-layer salinity is maximum in spring, with an amplitude of about 0.2. Precipitation, evaporation, advection and entrainment all played a role in the seasonal balance. Foltz and McPhaden (2008) looked at the seasonal variability of SSS in three regions in the Atlantic, one in the central North Atlantic with a weak seasonal cycle and two in the tropical Atlantic and Western North Atlantic with stronger ones.

Bingham et al. (2010; henceforth BFM) examined the seasonal cycle of SLS in the Pacific Ocean between 40° S and 60° N. They found areas with large seasonal variation

OSD
8, 2377–2415, 2011

in the northern tropical Pacific, under the ITCZ, along the western and northern boundary of the North Pacific, and in the central South Pacific loosely centered around 10° S. They compared these variations to the corresponding atmospheric forcings, evaporation (E), precipitation (P), and $E - P$. They also examined one of the advection terms and the entrainment term in the equation for SSS evolution. Both of these were usually not significant, and small where they were. The overall impression is that seasonal variations in SLS, where present, are mainly driven by seasonal variations in $E - P$. Even the amplitudes and phases matched in a few closely studied areas. This is not to say that advection, entrainment and other such processes are not important in the overall SLS balance, just they are generally not dominant on seasonal time scales.

While these previous efforts have been worthwhile, a global view of the seasonal cycle of SLS is called for in more detail than was provided by Boyer and Levitus (2002) or Roemmich and Gilson (2009). We need to know how well SLS and surface freshwater flux match on a global scale to help us better understand how ocean surface freshwater flux controls the global hydrologic cycle. We will therefore describe when and where the seasonal harmonic is important and how the seasonal amplitudes and phases fit into a global picture. We will compare the seasonal variability of SLS to that of evaporation and precipitation to get a sense of the relationship between them. We provide a quantification of the global seasonal cycle of SLS in relation to surface forcing, building on more qualitative previous analyses that were conducted before the Argo era.

2 Data

Salinity values used in this publication are unitless practical salinities based on the practical salinity scale of 1978 (UNESCO, 1981; Valladares et al., 2011). Table 1 shows the URLs where various datasets were accessed.

SLS is defined here as the uppermost salinity measurement in a given profile as long as it is above 10 m, or a single bucket or thermosalinograph measurement. It differs

OSD
8, 2377–2415, 2011

from SSS which can be considered a skin value within 1 cm of the surface (Henocq et al., 2009; Yu, 2010).

The SLS data come from Argo (http://www.argo.net; Table 1, line 1), the World Ocean Database (Table 1, line 2; Johnson et al., 2009), the Sea Surface Salinity Observation Service (Delcroix et al. (2005); LEGOS; Table 1, line 3) and the Global Surface Underway Data (http://www.gosud.org; GOSUD; Table 1, line 4) project. Argo data are profiling floats. The World Ocean Database is a compendium of historical data collected mainly by research vessels. LEGOS is a program to measure and archive data collected using buckets and thermosalinographs from volunteer observing ships from 30° S to 30° N during 1950–2003. Following Delcroix et al. (2005), we subtracted 0.1 from each bucket salinity value in the LEGOS dataset. GOSUD data are from thermosalinographs on board specially outfitted commercial vessels. These four data sources were combined and screened for duplicates. As explained in BFM (Sect. 2.1.6) no systematic quality control beyond that of the data providers was carried out due to the disparate nature of the data sources. Our final SLS dataset consists of 1.66×10^6 observations (Fig. 1) between about 60° S and 60° N (actually 61.25° S and 61.25° N). The number of observations increases with time (Fig. 2), with the exception of the mid-1990s, to nearly 100 000 yr^{-1} in 2010.

We note that there are many moorings associated with the Indian (RAMA), Pacific (TAO) and Atlantic (PIRATA) tropical arrays. No SLS data from any of these moorings are included here as the purpose of this study is to get a broad spatial view. Data from a similar SLS dataset and some TAO moorings were compared by BFM who found good agreement in seasonal amplitudes and phases.

Evaporation and precipitation data were obtained from the National Centers for Environmental Prediction (NCEP) Climate Forecast System Reanalysis (CFSR; Table 1, line 5; Saha et al., 2010). We used the monthly product in the date range January 1979–December 2009. This product is distributed on a 2.5° × 2.5° grid, which is also the size of the grid in which we did our calculations with the SLS data. A similar analysis was carried out in BFM for the Pacific using different flux products: the

OSD
8, 2377–2415, 2011

OAFlux dataset (Yu et al., 2008) for evaporation and the Global Precipitation Climatology Project (Adler et al., 2003) for precipitation. For the Pacific, the results from BFM (their Figs. 8 and 10) and those presented here are nearly identical. The amplitude and phase of the seasonal cycle computed (by harmonic analysis, see below) from these two datasets were compared by scatter plot (not shown) with those from the CFSR. Most points fell close to a one-to-one correspondence line, indicating that the results we will show do not depend on which of these flux products is used.

The mixed-layer depth climatology we used was derived from the World Ocean Database by de Boyer Montegut et al. (2004) (Table 1, line 6). It uses a temperature criterion of 0.2 °C difference from 10 m depth to estimate the mixed-layer depth. Note this is not a time series, but a seasonal climatology, with a single value for each month for each 2° square. The surface forcing term, $S_0(E-P)/h$ was calculated from the mixed-layer depth, E and P after interpolating them to a common $2.5^\circ \times 2.5^\circ$ grid. S_0 is a reference salinity (35) and h is the mixed-layer depth from the climatology.

The harmonic analysis we performed is detailed in BFM, Sect. 2.2 (see also Emery and Thomson, 2001, 392–397). The product is an amplitude and phase for SLS, E, P, $E-P$ and $S_0(E-P)/h$ in each $2.5^\circ \times 2.5^\circ$ grid box. The phase is expressed in months relative to 1 January of the maximum of each quantity. The amplitude is unitless for SLS, in units of $\mathrm{kg\,m^{-2}\,s^{-1}}$ for E, P and $E-P$ and $\mathrm{s^{-1}}$ (or $\mathrm{pss\,s^{-1}}$) for $S_0(E-P)/h$. ($S_0(E-P)/h$ was converted to units of $\mathrm{s^{-1}}$ by division of $(E-P)$ by the density of pure water, $1000\,\mathrm{kg\,m^{-3}}$). Note $1.0 \times 10^{-4}\,\mathrm{kg\,m^{-2}\,s^{-1}}$ is equivalent to $320\,\mathrm{cm\,yr^{-1}}$ of freshwater evaporation or precipitation. Since the amplitudes and phases were obtained using a common multivariate linear least squares procedure, the statistical significance could be easily evaluated using a standard F-test (e.g., Emery and Thomson, 2001, 254–257). Fits were considered significant if they were at or above the 95 % level.

OSD
8, 2377–2415, 2011

3 Results

Global values of SLS amplitude, phase and percent of variance are presented in Figs. 3, 4 and 5. Figures 3 and 4 are similar to a figure published by Boyer and Levitus (2002, their Fig. 3). The additional information here is that areas where the harmonic fit is not statistically significant no value is shown. Further, the harmonics here are obtained not from a gridded climatology, but from the observations themselves.

Areas having large amplitudes cluster in several regions: along 10° N and 5–10° S in the Atlantic, Pacific and Indian Oceans; Western Pacific marginal seas including the Indonesian Archipelago, South China Sea and Sea of Japan; the eastern boundary region of the Pacific and Atlantic equatorial ocean. The western and northern boundary of the North Pacific, and to a lesser extent the North Atlantic, contain a very large area with weak but significant seasonal cycles. There are large areas of the global ocean with no consistent seasonal cycle at all: most areas of the Southern Hemisphere below 20° S including the Southern Ocean; much of the central North Pacific and North Atlantic. If one calculates the actual surface area for each 2.5° × 2.5° square, and figures out which ones have a significant seasonal cycle, it amounts to about 37 % of the ocean surface between 60° S and 60° N, or 1.1×10^8 km^2.

The phase of the seasonal cycle shows consistent behavior across ocean basins (Fig. 4). The large bands across 10° N and 5–10° S have maximum SLS in each hemisphere's respective late spring, with the exception of the Arabian Sea where it is maximum in mid-summer. The western boundary areas in the North Pacific and North Atlantic are maximum in late winter. The percentage of variance (Fig. 5) indicates that the seasonal cycle accounts for a large fraction of the variance in the off-equatorial bands, particularly the ones in the Northern Hemisphere. Elsewhere, the percentage of variance is mostly smaller, with the exception of the Pacific marginal seas, particularly the Indonesian seas where it reaches 60–80 % of the variance.

If each individual 2.5° × 2.5° square is considered as an observation, then we can aggregate the observations to get a sense of the global distribution of the seasonal cycle.

OSD
8, 2377–2415, 2011

Figs. 6 and 7 display the distribution of the seasonal cycle amplitude and phase (blue bars). The amplitude peaks at 0.1–0.2, with the majority of areas below 0.5. The phase has a remarkable two-peaked distribution (Fig. 7). Most squares have maximum SLS in either March/April or September/October, with relatively few having maxima in December and July. Looking at the horizontal bars in Figs. 6 and 7 gives a sense of how the amplitude and phase is distributed by hemisphere. The peak in March/April is almost entirely determined by processes occurring in the Northern Hemisphere, whereas the one in September/October is mostly associated with the Southern Hemisphere. While the small amplitude seasonal cycles occur in both hemispheres, the large amplitude ones occur mostly in the northern (Fig. 6).

We did a calculation of frequency distribution of SLS phase and amplitude as shown in Figs. 6 and 7, only using total surface area instead of the simple number of $2.5^\circ \times 2.5^\circ$ squares. The total area of a $2.5^\circ \times 2.5^\circ$ square changes as a function of latitude and we wanted to make sure that this was not a major factor. The results are not shown here as they were very similar to the results we do show in Figs. 6 and 7.

Examining the Northern Hemisphere more closely (Figs. 8 and 9) we can see the distribution of amplitude and phase by latitude. The March/April peak (Fig. 8) is mainly determined by processes in in the 30–60° N range, while the lower latitudes peak about a month later in April/May. The September/October peak is exclusively a result of the 20–40° N latitude range, in particular the region centered at 30° N, 150° W (Fig. 3). In terms of amplitude (Fig. 9), areas with smaller amplitude are evenly distributed throughout the hemisphere, whereas areas with larger amplitudes are mainly in lower latitudes, 0–20° N.

When one looks more closely at the large amplitude areas of the Northern Hemisphere (Fig. 10), one can see that this is largely confined to lower latitudes, $< 30^\circ$ N, mainly the area under the ITCZ (Fig. 3).

The seasonal cycle of E, P, $E-P$ (Fig. 11) and $S_0(E-P)/h$ (Fig. 10) show many areas with significant seasonal cycles of $E-P$ where there are none of SLS (Fig. 3). The evaporation (Fig. 11c,d) has large amplitudes in the western boundary regions of

OSD
8, 2377–2415, 2011

the North Pacific and North Atlantic, and relatively small but consistent values elsewhere. The precipitation (Fig. 11e,f) has areas of activity under the ITCZ in the Atlantic and Pacific, in the western boundary region of the North Pacific (but not so much in the North Atlantic), in the Indonesian seas and in the Bay of Bengal. (Fig. 11e,f is similar to Adler et al., 2003, their Fig. 15.) When E and P are combined into $E-P$ (Fig. 12a,b), the result takes on most of the characteristics of P, except in the Western North Pacific and North Atlantic. In other words, in the areas of the ocean where there are seasonal cycles of $E-P$, they are mostly a result of P, with a couple of smaller areas associated with E. Finally, the term $S_0(E-P)/h$ the surface flux term in the salinity balance equation (see below). This term is similar in distribution to $E-P$ (Fig. 11a,b). The Northern Hemisphere western boundary regions, particularly in the North Pacific, appear as hot spots in amplitude. Large areas of the Southern Hemisphere oceans have no seasonal cycle of this term. The Southern Hemisphere western boundary regions have no counterpart to the Northern Hemisphere's, giving the impression of a Southern Hemisphere that is far less seasonal than the northern.

Taking Figs. 12 and 3 and 4, we can get some insight into the details of the relationship between $S_0(E-P)/h$ and SLS. First, we take all the $2.5^\circ \times 2.5^\circ$ squares depicted in Figs. 3 and 11 and extract only those squares where there is also a statistically significant value in both. We then do a scatter plot of amplitude (Fig. 13) and phase (Fig. 14) comparing the two. For the amplitude, generally the larger the amplitude of SLS is, the larger the amplitude of $S_0(E-P)/h$. This is a general trend however, and does not line up well on any straight line. In particular, the light line in Fig. 13 indicates the slope the data would have if SLS were simply related to $S_0(E-P)/h$ (see below). We find that for small $S_0(E-P)/h$ (less than $3\times10^{-8}\,\mathrm{s}^{-1}$) the amplitude of SLS is larger than expected based on this simple relationship, and for large $S_0(E-P)/h$ the amplitude of SLS is often smaller than expected. For the phase, there are two groupings of points in SLS, (March, April) and (September, October). Note these groupings match the frequency distribution of Figs. 6 and 7. The light line indicates where points would line up if the SLS were 3 months or 1/4 cycle behind $S_0(E-P)/h$. Notice that the SLS maximum

OSD
8, 2377–2415, 2011

generally comes earlier than this 1/4 cycle delay.

A simplified form of the same information is presented as a frequency distribution of $S_0(E-P)/h$ amplitude (Fig. 6, red bars) and phase (Fig. 7, red bars) and for the Northern Hemisphere at larger amplitudes (Fig. 8b). We can see that this quantity in a global sense leads the SLS by 1–2 months (Fig. 7), with maxima in January and July/August. The red bars show the surface flux at a maximum during the period when the ocean is getting saltier (January and July) and a minimum when it is getting fresher (May and November). This is consistent with winter months being a time of maximum evaporation in the western boundary regions of the Northern oceans. This strong wintertime evaporation is associated with mode water formation (e.g., Oka and Qiu, 2011).

Suppose that SLS (or S) on the seasonal time scale does not depend on advection, entrainment, or mixing and obeys this simple relationship between SLS and surface flux of freshwater (Delcroix et al., 1996)

$$\frac{\partial S}{\partial t} = \frac{S_0(E-P)}{h}. \tag{1}$$

To examine the seasonal component of this balance, let $S = A\sin(\omega t + \phi)$, where

$\omega = 2\pi$ radians/year $= 20 \times 10^{-8}$ s^{-1}

and ϕ is some arbitrary phase. In that case, we have

$$\frac{\partial S}{\partial t} = A\omega\cos(\omega t + \phi) = A\omega\sin\left(\omega t + \phi + \frac{\pi}{2}\right)$$

To make Eq. (1) balance, we need to have

$$\frac{S_0(E-P)}{h} = B\sin\left(\omega t + \phi + \frac{\pi}{2}\right)$$

where B is the amplitude of $S_0(E-P)/h$. The phase of $\frac{\pi}{2}$ represents a 1/4 cycle or three month delay between $S_0(E-P)/h$ and SLS as shown by the light line in Fig. 14.

OSD
8, 2377–2415, 2011

The frequency ω is the ratio of the amplitude of SLS and $S_0(E-P)/h$, B/A. This is the factor represented by the light line in Fig. 14. The discrepancies between the scatter of points in Figs. 13 and 14 and the light lines indicates that while surface flux is an important element in producing the seasonal cycle of SLS, it is not the complete story. In most cases, the SLS maximum comes a month or two too early. (The same scatter plots were made with just $E-P$, with similar results.) BFM looked at four examples of areas in the Pacific and compared dS/dt with $S_0(E-P)/h$ (their Table 1). They found similar results showing that dS/dt peaks about a month to two earlier than would be expected if completely balanced by $S_0(E-P)/h$ in three of the areas. What we have shown here is that this appears to be the case over much of the globe.

The average amplitude as a function of latitude (Fig. 15) compares SLS and $S_0(E-P)/h$ in a less detailed way. In this calculation, amplitudes were averaged in 10° latitude bands. The highest amplitudes are just north of the equator, demonstrating the much more seasonal nature of the Northern Hemisphere. If Eq. (1) were true one would expect the values from the red curve to fall on top of the blue curve. This is close to being the case for the Northern Hemisphere between 25 and 45° N and also for the Southern Hemisphere at 15 and 25° S. When the two curves do not fall on top of each other and the blue curve is above the red curve, the SLS amplitude is too large to be driven by surface flux alone.

We can take the difference between the amplitude of SLS and $S_0(E-P)/h$ to see where the two are out of balance and by how much (Fig. 16). This difference shows that the imbalance is less than $5.0\times10^{-8}\,\mathrm{s}^{-1}$ ($0.1\,\mathrm{month}^{-1}$) over much of the globe. In much of the vast area of the North Pacific along the western and northern boundary dominated by evaporation, the figure shows that the difference between the terms is not statistically significant. It is borderline significant in the rest of the area. This is also the case in other areas, the eastern tropical Pacific, the eastern North Atlantic, much of the South Pacific and South Atlantic. There are a few areas where the difference is significant, and the amplitude of SLS is too large to be explained by $S_0(E-P)/h$ (blue color): (1) parts of the eastern tropical Atlantic and Pacific, specifically the Gulf of Guinea and

OSD
8, 2377–2415, 2011

the coast of Ecuador; (2) the Arabian Sea; (3) Indonesian Seas and South China Sea; (4) the coast of Labrador and entrance to the Labrador Sea; (5) the North Brazil coast; 96) the central Pacific ITCZ. In (1), near Africa, this corresponds to the outflow of the Congo River which could have some influence. Its discharge peaks twice per year, in March and October (Dai and Trenberth, 2002). The area near Ecuador could be influenced by seasonal moisture transport across Central America, which peaks in August (Rasmussen, 1967). In (2), the area corresponds to that documented by Rao and Sivakumar (2003), who attributed the large seasonal cycle there to advection during the summer monsoon season. For (3), perhaps continental or island runoff are the cause. In (4) the area is affected by freshwater export by the Labrador Current (Schmidt and Send, 2007; Straneo, 2006). This export peaks in summer, which matches the cycle of SLS, which peaks in wintertime. Along the north coast of Brazil, (5), the enhanced seasonal cycle is likely to be a result of seasonal changes in runoff from the Amazon River (Hellweger and Gordon, 2002; Romanova et al., 2011) whose discharge peaks in May or June (Dai and Trenberth, 2002). Again this matches the SLS, which peaks in winter. For the Pacific ITCZ, (6), BFM showed that seasonal advection of the mean salinity gradient was a significant part of the seasonal SLS dynamics, where seasonally-varying zonal currents cross a meridionally sloping mean salinity gradient. There are areas where the SLS amplitude is too small to match $S_0(E-P)/h$ (red shading), near Central America and West Africa. This could be due to damping of the SLS signal by advection or entrainment.

We examined the $2.5^\circ \times 2.5^\circ$ squares where there were seasonal cycles of $S_0(E-P)/h$, but not SLS, that is, areas where there was atmospheric forcing with a seasonal component, but no corresponding seasonal variability in the ocean. In these squares, the amplitude of the surface forcing tended to be smaller than for squares with oceanic variability. The median value of amplitude of $S_0(E-P)/h$ for squares with no corresponding oceanic seasonal cycle is $1.3 \times 10^{-8}\,\mathrm{s}^{-1}$. For squares with an oceanic seasonal cycle, the median value is $2.5 \times 10^{-8}\,\mathrm{s}^{-1}$ (see Fig. 6). Another way of saying this is that the weaker the surface forcing, the less likely an area is to have a significant

OSD
8, 2377–2415, 2011

seasonal cycle of SLS. This fits with the general picture of the seasonal variability of SLS being mostly controlled by $S_0(E-P)/h$.

4 Discussion

The frequency distribution of Fig. 7 implies a significant semi-annual transfer of water from ocean to atmosphere or horizontally within the ocean. Areas of the ocean that have a high salinity in March lose net freshwater between the months of September and March and gain freshwater between March and September (in the absence of other processes to alter SLS). Presumably this water leaving the ocean during the (northern) fall and winter moves somewhere else during that period. Perhaps it is transported to the atmosphere and land surface, or to some other part of the ocean.

To get a sense of how large that transfer might be, we can do a rough calculation. Suppose that the area with maximum salinity in March/April is comprised of 500 $2.5^\circ \times 2.5^\circ$ squares and that these squares experience a seasonal cycle of amplitude 0.19, the median value of SLS amplitudes (Fig. 14). Also suppose that this occurs over a mixed-layer depth of typically 50 m and that a $2.5^\circ \times 2.5^\circ$ square has an area of 250^2 km^2. To go through a change of this magnitude, these squares would have to lose and gain an average amount of water equivalent to 60 cm each year. Multiplying by the surface area, this comes out to a yearly transfer of freshwater of about 19×10^3 km^3, larger than the total atmospheric content of about 13×10^3 km^3 (Trenberth and Guillemot, 1994) and much larger than the seasonal cycle of water vapor content in the atmosphere which is about 1.0×10^3 km^3 (Trenberth et al., 1988). For such a large ocean-atmosphere exchange of freshwater to occur, there must be a significant pathway for freshwater to get from one place to another during the course of a year, with the atmosphere being the obvious candidate. The frequency distribution of Fig. 7 and distribution map of Fig. 4 imply that this pathway leads from the Northern Hemisphere under the ITCZ and along the northern and western boundary of the North Pacific and North Atlantic where SLS peaks in March, to the Southern Hemisphere and the eastern

OSD
8, 2377–2415, 2011

North Pacific and North Atlantic where SLS peaks in September and October. The land surface also plays a part by storing water (Ramillien et al., 2005). The Northern Hemisphere atmosphere contains more moisture during the boreal summer months than the winter due to higher temperature (Sun and Oort, 1995). This is consistent with atmospheric moisture transport from southern to Northern Hemisphere during boreal summer.

The difference between the maxima in September and March from Fig. 7 implies that the ocean contains more mass during September than it does in March. This agrees with a study of net oceanic mass from satellite altimetry (Minster et al., 1999) which shows a maximum of oceanic mass in mid-September equivalent to 9.5 mm of sea level height above a minimum value, and a study of satellite gravity measurements (Chambers et al., 2004) which shows a maximum of oceanic mass in mid-October equivalent to 8.5 mm of sea level height. A 9.5 mm height difference is equivalent to a globalized average SLS amplitude of 0.02 when spread over a 50 m mixed-layer. Taking our median amplitude, 0.19, and multiplying it by the 37 % of the surface of the ocean between 60° S and 60° N that has an identifiable SLS seasonal cycle, you get a globalized value of 0.06, which has the same order of magnitude, though is somewhat larger.

The results shown here indicate that the seasonal cycle of SLS is in most places in rough balance with input and export of freshwater at the ocean surface through evaporation and precipitation. A typical imbalance has a magnitude of less than 5.0×10^{-8} s^{-1} (Fig. 16). This is the case throughout the evaporation-dominated regime of the mid-latitude North Pacific along the western and northern boundary. Areas with larger imbalances than that correspond to places where one might expect them to exist, e.g. the vicinity of the Amazon River plume, the monsoon-influenced Arabian Sea and to a lesser extent the ITCZ.

This is not the complete picture though. Figure 13 indicates that the size of the seasonal cycle of SLS is in most places larger than would be expected by surface forcing alone. This mismatch is especially noticeable in the tropics (Figs. 10 and 15). Perhaps

OSD
8, 2377–2415, 2011

this is due to vertical mixing as the top of the thermocline is eroded in winter or restratified in summer. In areas of the subtropical and tropical oceans equatorward of the great horizontal salinity maxima where the subtropical underwater outcrops (Bingham and Suga, 2002; O'Connor et al., 2002, 2005), salinity increases downward at the base of the mixed layer towards the shallow salinity maximum (Suga et al., 2000). So as the mixed layer increases in thickness during winter, saltier water is mixed into the surface layer. This is consistent with the prevalence of high salinity in the late winter seen in Fig. 7. This is not the case however poleward of the central horizontal salinity maxima where salinity decreases with depth. Though we have not attempted to estimate the term here, the scatter plot of Fig. 13 gives an idea of how large it might be.

The mystery that this analysis leaves us with is shown in Figs. 7 and 13, that is, the shortened phase delay between SLS and $S_0(E-P)/h$. Why does this delay seem to be 1–2 months shorter than we would expect, consistent across ocean basins and regimes? A couple of possible explanations present themselves. We have done a harmonic analysis here, which assumes that the signal is in the form of a sine function. SLS is controlled by physical processes that do vary in a smooth, sinusoidal way. A full Fourier decomposition of the SLS might find semi-annual or bi-annual or other components that could skew the seasonal cycle, turning it into, say, a sawtooth-like form rather than a symmetric sine either for SLS or $S_0(E-P)/h$, or both. One could imagine this being the case for an area of the ocean that is subject to a single season of very intense rainfall with much less surface or other input of freshwater at other times of year.

Another possible explanation involves the idea that we have looked at SLS, that is the near-surface salinity. There has been a lot of attention in recent years paid to barrier layers (Sato et al., 2004, 2007; de Boyer Montegut et al., 2004), low salinity layers that occupy the upper water column and inhibit vertical mixing (Lukas and Lindstrom, 1991). The presence of a barrier layer may shorten the time it takes the surface salinity to react to an impulsive atmospheric input of freshwater. So Figs. 7 and 13 may reflect the effect of barrier layers that shorten the response time of SLS to seasonal forcing.

OSD
8, 2377–2415, 2011

Whatever the explanation of this discrepancy, it is likely that the too large amplitudes and the too short phase delays (Figs. 6, 7, 13 and 14) are related.

We have not tried to quantify the contribution of advection, entrainment or mixing to the annual cycle of SLS. BFM did show that the advection and entrainment terms were small in the Pacific basin, except for an area in the tropical Pacific equatorward of 15°. The SLS could also be balanced by input of salt or freshwater to the surface layer at some other time scale, whether by advection, mixing, entrainment, surface flux or some other process. As an example of such a time scale, El Nino events are phase-locked to the seasons and may produce variability of surface properties that, while seasonal in nature, are not produced by physical processes that are fundamentally seasonal. BFM did a similar calculation as shown in Fig. 3 controlling for the El Nino phase, and got similar results for the Pacific basin. The one process that we have not looked at in this study is vertical mixing, which would be very likely to have a seasonal component. As the mixed-layer increases and decreases in size over the course of the year, it incorporates freshwater and/or salt from the layer below. This would be especially strong in areas of deep convection, formation areas of mode, intermediate or deep water. How much this might contribute to the seasonal signal of SLS is a subject for future study.

With the recent launches of Aquarius and SMOS, the seasonal patterns displayed here will be a crucial test of the validity of those datasets. The satellites should measure seasonal cycles of roughly the same amplitude, phase and distribution as shown in Figs. 3–5. The hope is that the satellite measurements will add much more detail to those pictures. BFM for example looked at advection of the mean SLS by the seasonally-varying current, but not advection of the seasonal SLS by the mean current. There is not any way to estimate the latter with currently available data. However, with the satellite measurements coming available, this should become possible. While the salinity balance of the upper ocean is still not well-understood, the contribution of advection and mixing to the balance, whether seasonal or otherwise, will become clearer as these new observations come online.

OSD
8, 2377–2415, 2011

Acknowledgements. The GOSUD surface data were collected in the framework of national programmes. They are aggregated and made freely available in the frame of the GOSUD Project: http://www.gosud.org. Argo data were collected and made freely available by the International Argo Project and the national initiatives that contribute to it (http://www.argo.net). Argo is a pilot programme of the Global Ocean Observing System. FMB was supported by NASA under grants NNX09AU70G and NNX11AE83G.

References

Adler, R. F., Huffman, G. J., Chang, A., Ferraro, R., Xie, P., Janowiak, J., Rudolf, R., Schneider, U., Curtis, S., Bolvin, D., Gruber, A., Susskind, J., Arkin, A., and Nelkin, E.: The version 2 Global Precipitation Climatology Project (GPCP) monthly precipitation analysis (1979 – present), J. Hydrometeorol., 4, 1147–1167, 2003.

Bengtsson, L.: The global atmospheric water cycle, Environ. Res. Lett., 5, 025202, doi:10.1088/1748-9326/5/2/025202, 2010.

Berger, M., Camps, A., Font, J., Kerr, Y., Miller, J., Johannessen, J., Boutin, J., Drinkwater, M. R., Skou, N., Floury, N., Rast, M., Rebhan, H., and Attema, E.: Measuring ocean salinity with ESA's SMOS mission, ESA Bull.-Eur. Space, 111, 113–121, 2002.

Bingham, F. and Lukas, R.: Seasonal cycles of temperature, salinity and dissolved oxygen observed in the Hawaii Ocean time-series, Deep-Sea Res. Pt. II, 43, 199–213, 1996.

Bingham, F. M., Suga, T., and Hanawa, K.: The origin of waters observed along 137° E, J. Geophys. Res., 107, 3073, doi:10.1029/2000jc000722, 2002.

Bingham, F. M., Foltz, G. R., and McPhaden, M. J.: Seasonal cycles of surface layer salinity in the Pacific Ocean, Ocean Sci., 6, 775–787, doi:10.5194/os-6-775-2010, 2010.

Boyer, T. P. and Levitus, S.: Harmonic analysis of climatological sea surface salinity, J. Geophys. Res.-Oceans, 107, 8006, doi:10.1029/2001JC000829, 2002.

Boyer, T. P., Levitus, S., Antonov, J., Conkright, M., O'Brien, T., and Stephens, C.: World Ocean Atlas 1998 Volume 4: Salinity of the Atlantic Ocean, NOAA Atlas NESDIS 30, US Gov. Printing Office, Wash., D.C., 1998a.

Boyer, T. P., Levitus, S., Antonov, J., Conkright, M., O'Brien, T., and Stephens, C.: World Ocean Atlas 1998 Volume 5: Salinity of the Pacific Ocean, NOAA Atlas NESDIS 31, US Gov. Printing Office, Wash., D.C., 1998b.

OSD

8, 2377–2415, 2011

Boyer, T. P., Levitus, S., Antonov, J., Conkright, M., O'Brien, T., and Stephens, C.: World Ocean Atlas 1998 Volume 6: Salinity of the Indian Ocean, NOAA Atlas NESDIS 32, US Gov. Printing Office, Wash., D.C., 1998c.

de Boyer Montégut, C., Madec, G., Fischer, A. S., Lazar, A. and Iudicone, D.: Mixed layer depth over the global ocean: An examination of profile data and a profile – based climatology, J. Geophys. Res., 109, C12003, doi:10.1029/2004JC002378, 2004.

Chambers, D. P., Wahr, J., and Nerem, R. S.: Preliminary observations of global ocean mass variations with GRACE, Geophys. Res. Lett., 31, 13310, doi:10.1029/2004GL020461, 2004.

Dai, A. and Trenberth, K. E.: Estimates of freshwater discharge from continents: latitudinal and seasonal variations, J. Hydrometeorol, 3, 660, doi:10.1175/1525-7541(2002)003<0660:EOFDFC>2.0.CO;2, 2002.

da Silva, A. A., Young, A. C., and Levitus, S.: Atlas of Surface Marine Data 1994, Vol. I, Algorithms and Procedures, NOAA Atlas, NESDIS 6, Washington, DC, 1994.

Delcroix, T. and Henin, C.: Seasonal and interannual variations of sea surface salinity in the Tropical Pacific Ocean, J. Geophys. Res., 96, 22135–22150, 1991.

Delcroix, T., Henin, C., Porte, V., and Arkin, P.: Precipitation and sea-surface salinity in the tropical Pacific, Deep-Sea Res. Pt. I, 43, 1123–1141, 1996.

Delcroix, T., McPhaden, M., Dessier, A., and Gouriou, Y.: Time and space scales for sea surface salinity in the tropical oceans, Deep-Sea Res., 52, 787–813, 2005.

Dessier, A. and Donguy, J. R.: The sea surface salinity in the Tropical Atlantic between 10 degree S and 30 degree N – seasonal and interannual variations (1977–1989), Deep-Sea Res., 41, 81–100, 1994.

Durack, P. J. and Wijffels, S.: Fifty-year trends in global ocean salinities and their relationship to broad-scale warming, J. Climate, 23, 4342, doi:10.1175/2010JCLI3377.1, 2010.

Emery, W. J. and Thomson, R. E.: Data Analysis Methods in Physical Oceanography, Second and Revised Edition, Elsevier Science Ltd., Oxford, UK, 2001.

Foltz, G. R. and McPhaden, M. J.: Seasonal mixed layer salinity balance of the tropical North Atlantic Ocean, J. Geophys. Res., 113, C02013, doi:10.1029/2007JC004178, 2008.

Foltz, G. R., Grodsky, S. A., Carton, J. A., and McPhaden, M. J.: Seasonal salt budget of the northwestern tropical Atlantic Ocean along 38° W, J. Geophys. Res.-Oceans, 109, C03052, doi:10.1029/2003JC002111, 2004.

Gouriou, Y. and Delcroix, T.: Seasonal and ENSO variations of sea surface salinity and temperature in the South Pacific convergence zone during 1976–2000, J. Geophys. Res.-Oceans,

OSD
8, 2377–2415, 2011

107, 8011, doi:10.1029/2001JC000830, 2002.
Hellweger, F. L. and Gordon, A.: Tracing Amazon River water into the Caribbean Sea, J. Mar. Res., 60, 537–549, 2002.
Henocq, C., Boutin, J., Petitcolin, F., Reverdin, G., Arnault, S., and Lattes, P.: Vertical variability of near-surface salinity in the tropical: consequences for L-band radiometer calibration and validation, J. Atmos. Ocean. Tech., 27, 192, doi:10.1175/2009JTECHO670.1, 2009.
Johnson, D. R., Boyer, T. P., Garcia, H. E., Locarnini, R. A., Baranova, O., and Zweng, M. M.: World Ocean Database 2009 Documentation, NODC Internal Report 20, NOAA Printing Office, Silver Spring, MD, 175 pp., 2009.
Johnson, E., Lagerloef, G. S., Gunn, J., and Bonjean, F.: Surface salinity advection in the tropical oceans compared with atmospheric freshwater forcing: a trial balance, J. Geophys. Res., 107, 8014, doi:10.1029/2001JC001122, 2002.
Lagerloef, G. S., Colomb, F. R., Le Vine, D. M., Wentz, F., Yueh, S., Ruf, C., Lilly, J., Gunn, J., Chao, Y., deCharon, A., Feldman, G., and Swift, C.: The Aquarius/SAC-D mission: designed to meet the salinity remote-sensing challenge, Oceanography, 20, 68–81, 2008.
Lukas, R. and Lindstrom, E.: The mixed layer of the Western Equatorial Pacific, J. Geophys. Res., 96 (suppl.), 3343–3357, 1991.
Minster, J. F., Ceznave, A., Serafini, Y. V., Mercier, F., Gennero, M. C., and Rogel, P.: Annual cycle in mean sea level from Topex–Poseidon and ERS-1: inference on the global hydrological cycle, Global Planet. Change, 20, 57, doi:10.1016/S0921-8181(98)00058-7, 1999.
O'Connor, B. M., Fine, R., Maillet, K. A., and Olson, D. B.: Formation rates of subtropical underwater in the Pacific Ocean, Deep-Sea Res. Pt. I, 49, 1571, doi:10.1016/S0967-0637(02)00087-0, 2002.
O'Connor, B. M., Fine, R., and Olson, D.: A global comparison of subtropical underwater formation rates, Deep-Sea Res. Pt. I, 52, 1569, doi:10.1016/j.dsr.2005.01.011, 2005.
Oka, E. and Qiu, B.: Progress of North Pacific mode water research in the past decade, J. Oceanogr., doi:10.1007/s10872-011-0032-5, 2011.
Ramillien, G., Frappart, F., Ceznave, A., and Gunter, A.: Time variations of land water storage from an inversion of 2 years of GRACE geoids, Earth Planet. Sc. Lett., 235, 283, doi:10.1016/j.epsl.2005.04.005, 2005.
Rao, R. R. and Sivakumar, R.: Seasonal variability of sea surface salinity and salt budget of the mixed layer of the north Indian Ocean, J. Geophys. Res.-Oceans, 108, 3009, doi:10.1029/2001JC000907, 2003.

OSD
8, 2377–2415, 2011

Rasmussen, E. M.: Atmospheric water vapor transport and the water balance of North America: Part I: Characteristics of the water vapor flux field, Mon. Weather Rev., 95, 403, doi:10.1175/1520-0493(1967)095<0403:AWVTAT>2.3.CO;2, 1967.
Ren, L. and Riser, S.: Seasonal salt budget in the northeast Pacific Ocean, J. Geophys. Res.-Oceans, 114, C12004, doi:10.1029/2009JC005307, 2009.
Roemmich, D. and Gilson, J.: The 2004–2008 mean and annual cycle of temperature, salinity, and steric height in the global ocean from the Argo Program, Prog. Oceanogr., 82, 81, doi:10.1016/j.pocean.2009.03.004, 2009.
Romanova, V., Köhl, A., and Stammer, D.: Seasonal cycle of near-surface freshwater budget in the western tropical Atlantic, J. Geophys. Res.-Oceans, 116, C07009, doi:10.1029/2010JC006650, 2011.
Saha, S., Moorthi, S., Pan, H., Wu, X., Wang, J., Nadiga, S., Tripp, P., Kistler, R., Woollen, J., Behringer, D., Liu, H., Stokes, D., Grumbine, R., Gayno, G., Wang, J., Hou, Y., Chuang, H., Juang, H. H., Sela, J., Iredell, M., Treadon, R., Kleist, D., Van Delst, P., Keyser, D., Derber, J., Ek, M., Meng, J., Wei, H., Yang, R., Lord, S., Van, D. D., Kumar, A., Wang, W., Long, C., Chelliah, M., Xue, Y., Huang, B., Schemm, J., Ebisuzaki, W., Lin, R., Xie, P., Chen, M., Zhou, S., Higgins, W., Zou, C., Liu, Q., Chen, Y., Han, Y., Cucurull, L., Reynolds, R. W., Rutledge, G., and Goldberg, M.: The NCEP climate forecast system reanalysis, B. Am. Meteorol. Soc., 91, 1015–1057, 2010.
Sato, K., Suga, T., and Hanawa, K.: Barrier layer in the North Pacific subtropical gyre, Geophys. Res. Lett., 31, 5301, doi:10.1029/2003GL018590, 2004.
Sato, K., Suga, T., and Hanawa, K.: Barrier layers in the subtropical gyres of the world's oceans, Geophys. Res. Lett., 33, L08603, doi:10.1029/2005GL025631, 2007.
Schmidt, S. and Send, U.: Origin and composition of seasonal labrador sea freshwater, J. Phys. Oceanogr., 37, 1445–1454, 2007.
Straneo, F.: Heat and freshwater transport through the central labrador sea, J. Phys. Oceanogr., 36, 606–628, 2006.
Suga, T., Kato, A., and Hanawa, K.: North Pacific tropical water: its climatology and temporal changes associated with the climate regime shift in the 1970s, Prog. Oceanogr., 47, 223–256, 2000.
Sun, D. and Oort, A. H.: Humidity-temperature relationships in the Tropical Troposphere, J. Climate, 8, 1974–1987, 1995.
Tomczak, M.: Salinity variability in the surface layer of the tropical Western Pacific Ocean, J.

OSD
8, 2377–2415, 2011

Geophys. Res., 100, 20499–20515, 1995.
Trenberth, K. E. and Guillemot, C. J.: The total mass of the atmosphere, J. Geophys. Res.-Atmos., 99, 23079–23088, doi:10.1029/94JD02043, 1994.
Trenberth, K. E., Christy, J. R., and Olson, J. G.: Global atmospheric mass, surface pressure, and water vapor variations, J. Geophys. Res.-Atmos., 92, 14815, doi:10.1029/JD093iD09p10925, 1988.
UNESCO: Tenth Report of the Joint Panel on Oceanographic Tables and Standards, Unesco Technical Papers in Marine Science 36, Paris, 1981.
Valladares, J., Fennel, W., and Morozov, E.: Replacement of EOS-80 with the International Thermodynamic Equation of Seawater – 2010 (TEOS-10), Deep-Sea Res. Pt. I, 58, 978, doi:10.1016/j.dsr.2011.07.005, 2011.
Yu, L.: On sea surface salinity skin effect induced by evaporation and implications for remote sensing of ocean salinity, J. Phys. Oceanogr., 40, 85, doi:10.1175/2009JPO4168.1, 2010.
Yu, L., Jin, X., and Weller, R.: Multidecade Global Flux Datasets from the Objectively Analyzed Air-sea Fluxes (OAFlux) Project: Latent and Sensible Heat Fluxes, Ocean Evaporation, and Related Surface Meteorological Variables, Woods Hole Oceanographic Institution, OA Flux Project Tech Rept. OA-2008–01, 64 pp., Woods Hole, MA, 2008.

OSD
8, 2377–2415, 2011

Table 1.

	Dataset name	URL Accessed from	Date of most recent observation used in this paper
1	Argo	http://www.nodc.noaa.gov/argo/basins_data.htm	Aug 2011
2	World Ocean Database	http://www.nodc.noaa.gov/OC5/WOD/pr_wod.html	Dec 2004
3	LEGOS	http://www.legos.obs-mip.fr/en/observations/sss/datadelivery/products/	Jul 2003
4	GOSUD	http://www.gosud.org/Data-delivery/FTP-access	Mar 2009
5	NCEP CFSR	http://dss.ucar.edu/pub/cfsr.html	Dec 2009
6	Ocean Mixed-layer Climatology	http://www.locean-ipsl.upmc.fr/~cdblod/mld.html	N/A

OSD
8, 2377–2415, 2011

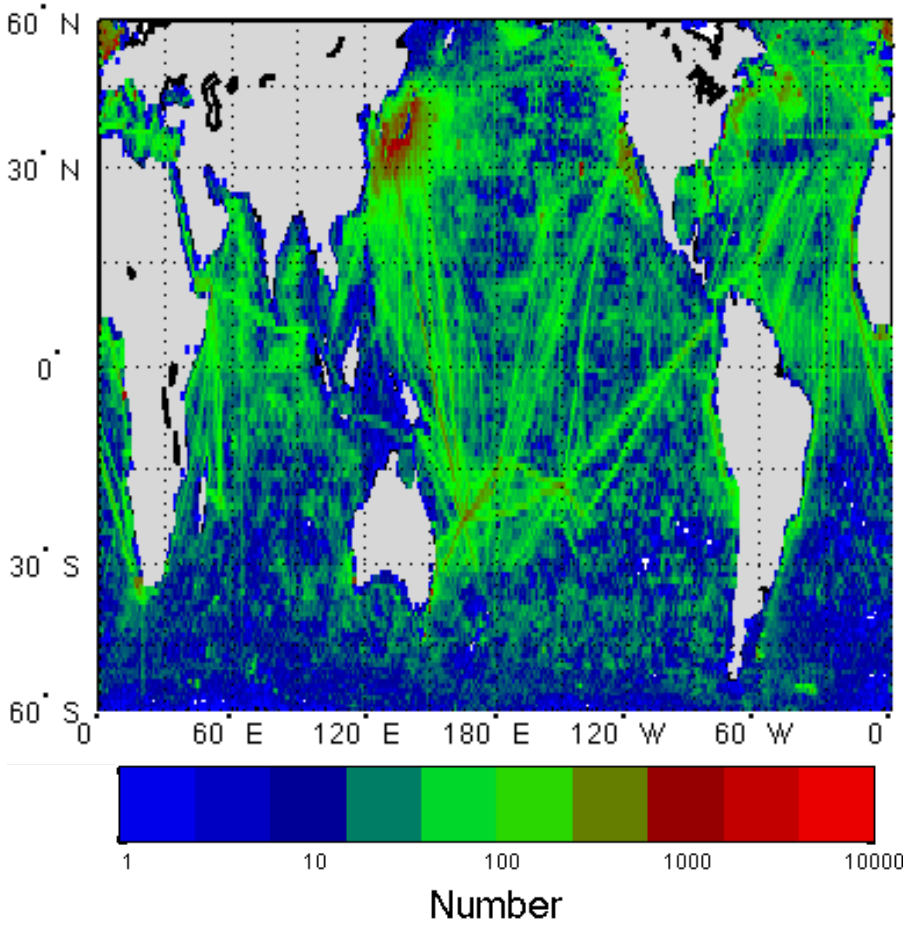

Fig. 1. Distribution of final SLS dataset in number of observations per $1^{\circ} \times 1^{\circ}$ square. Note this is the distribution of the final dataset after screening for duplicates.

OSD
8, 2377–2415, 2011

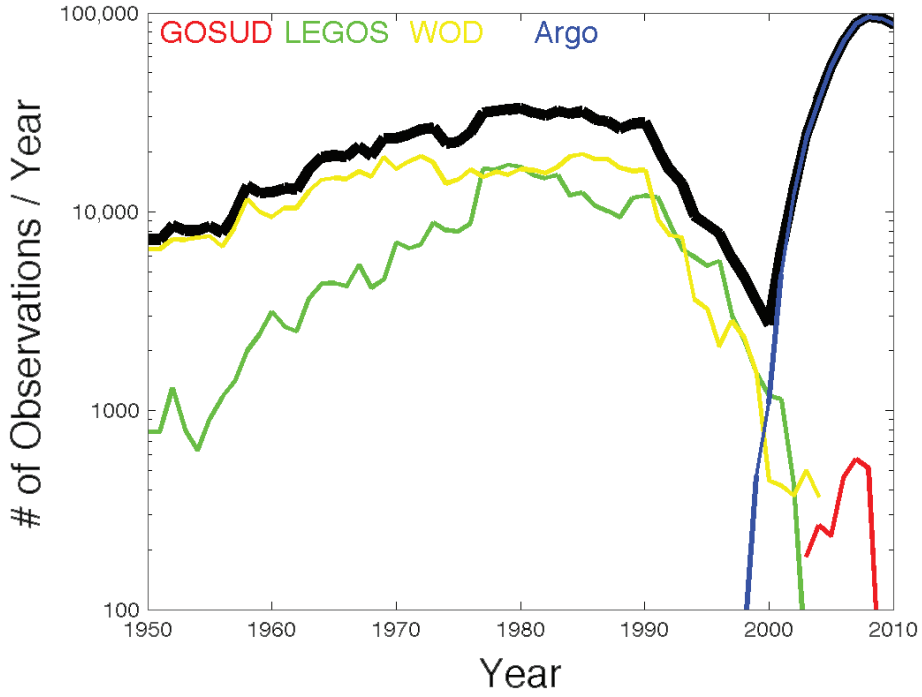

Fig. 2. Distribution of final SLS dataset by time. Colors of lines indicate different datasets as matched with colored text in the upper part of the figure. Dark black line is the total number of observations. Note this is the distribution of the final dataset after screening for duplicates. Note also the *y*-axis is logarithmic.

OSD
8, 2377–2415, 2011

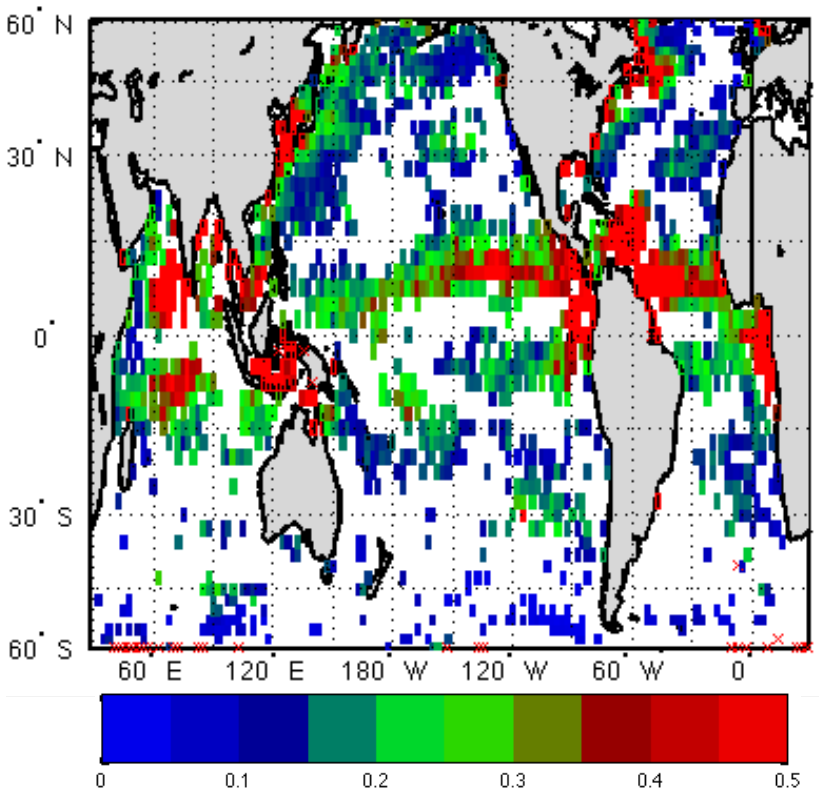

Fig. 3. Amplitude (unitless practical salinity) of the seasonal cycle of SLS in 2.5° × 2.5° squares. Ocean areas with no color had sufficient observations, but were found to have no significant seasonal cycle using a standard statistical test (see text for details). Areas with a red "×" have fewer than 10 observations. The scale indicates the numerical values associated with each color.

OSD
8, 2377–2415, 2011

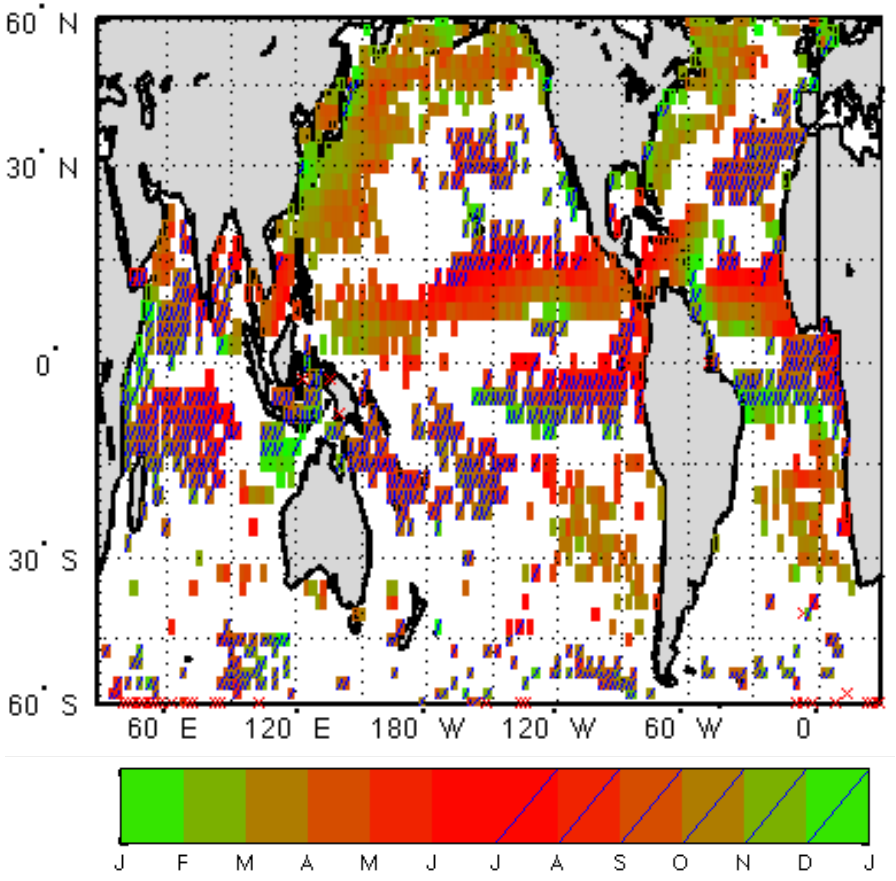

Fig. 4. As in Fig. 3, for phase (in months) indicating month of maximum SLS in each 2.5° × 2.5° square.

OSD
8, 2377–2415, 2011

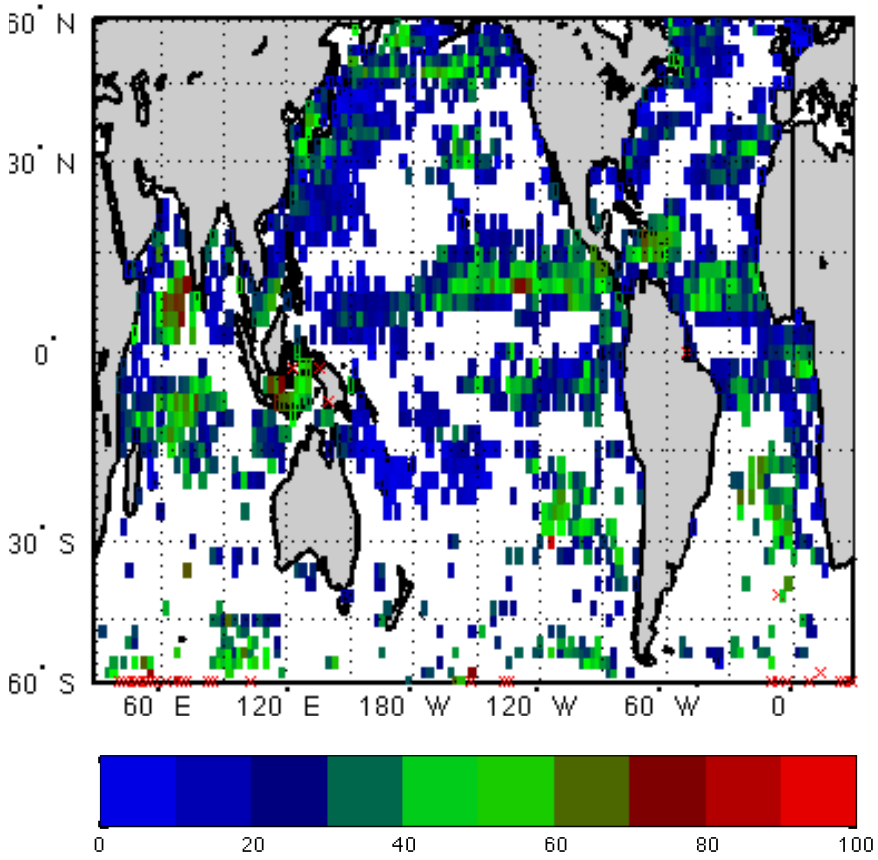

Fig. 5. As in Fig. 3, for R-squared (in %).

OSD
8, 2377–2415, 2011

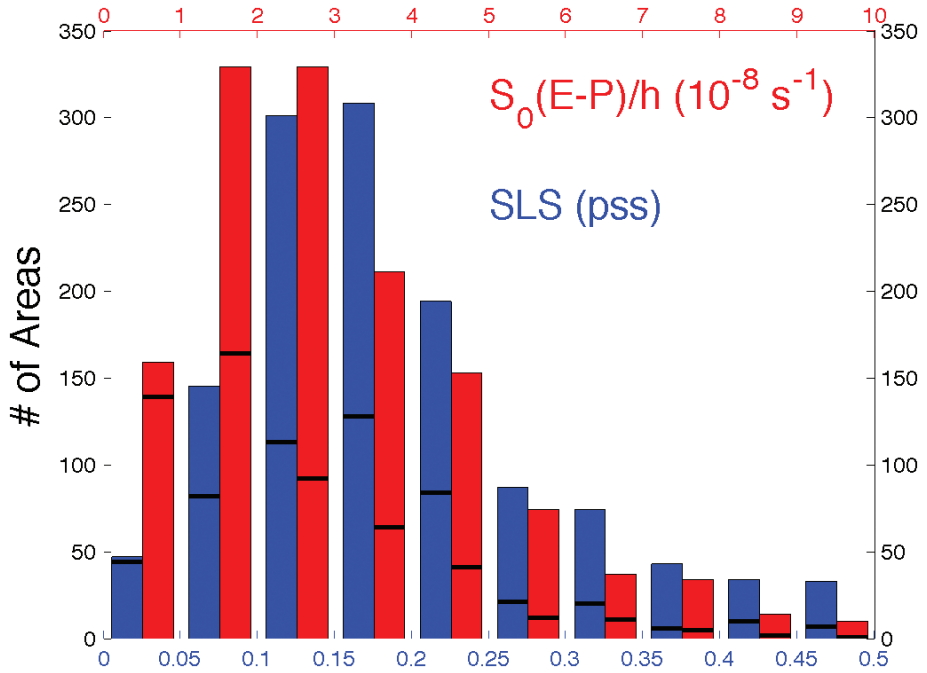

Fig. 6. Frequency distribution of the amplitude of SLS (blue bars) and $S_0(E-P)/h$ (red bars). The ordinate is the number of $2.5^\circ \times 2.5^\circ$ areas in the global ocean with amplitude in a given range. Units for the abscissa are given by red and blue text in the upper part of the figure. Black horizontal bars divide the number of areas in the Southern Hemisphere below the bars from the number in the northern.

OSD
8, 2377–2415, 2011

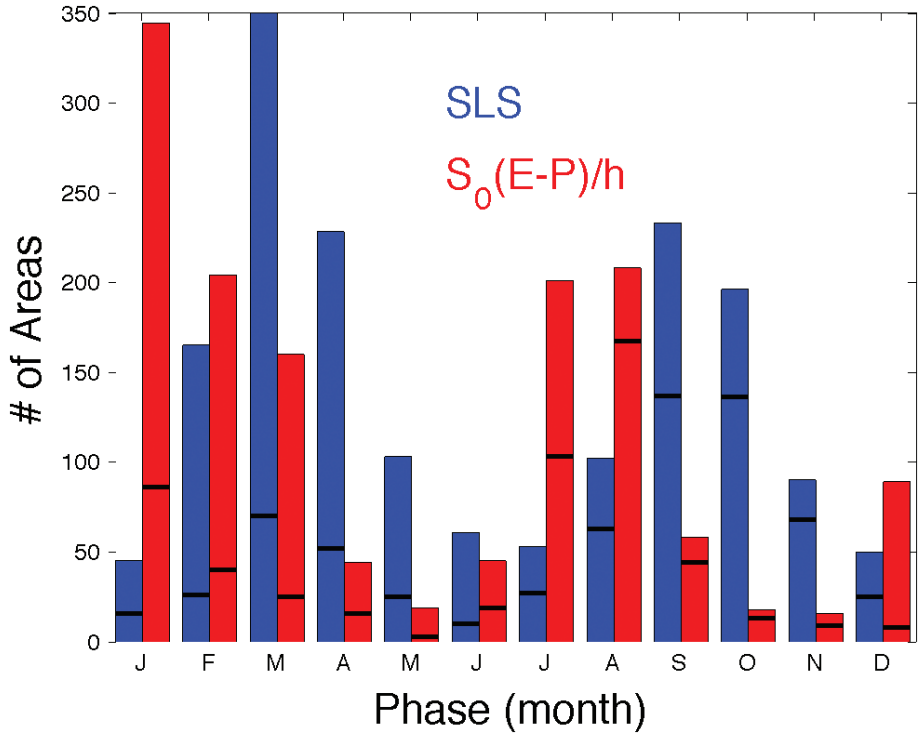

Fig. 7. As in Fig. 6, but for phase in months.

OSD
8, 2377–2415, 2011

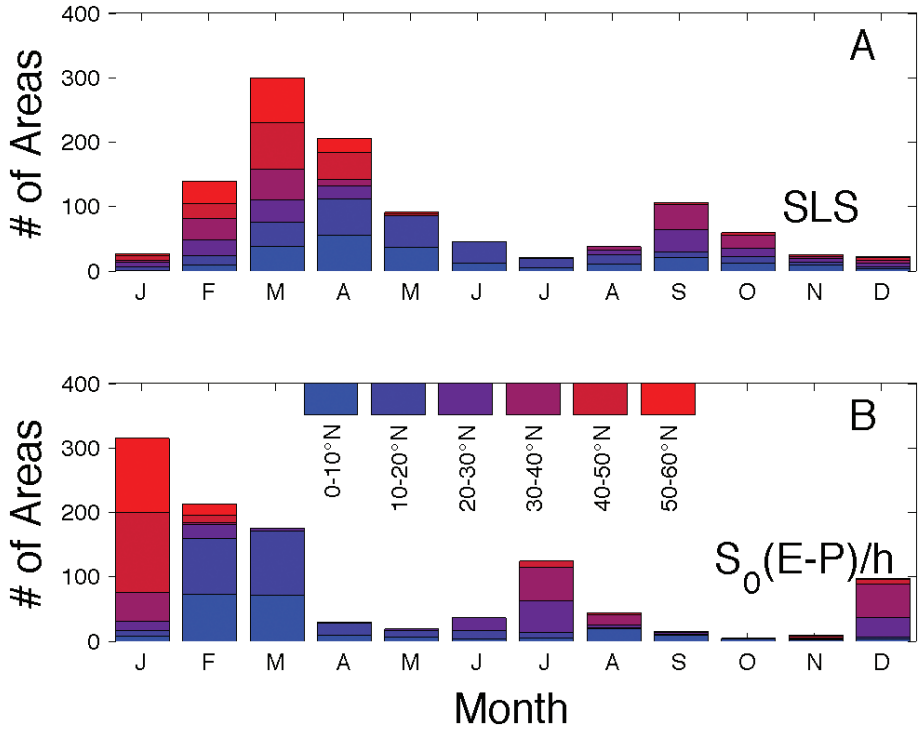

Fig. 8. (A) Frequency distribution of phase of SLS in the Northern Hemisphere only. Numbers on the *y*-axis represent a number of 2.5° × 2.5° squares with a particular value. Different colors represent different latitude ranges, with a color scale shown at top of panel **(B)**. **(B)** The same, but for $S_0(E-P)/h$ instead of SLS.

OSD
8, 2377–2415, 2011

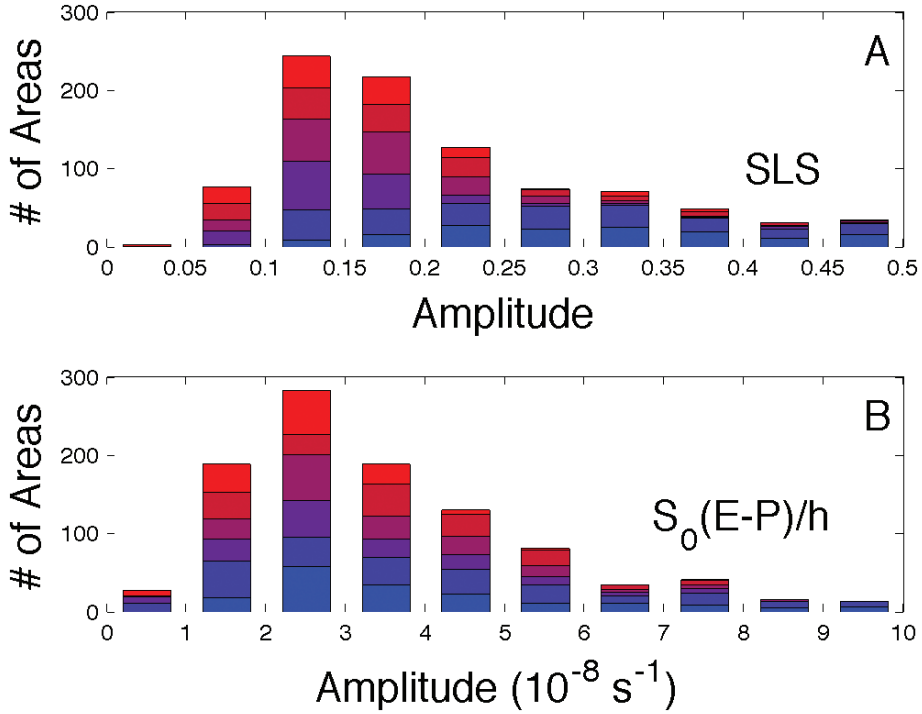

Fig. 9. As in Fig. 8, but for amplitude instead of phase. Color scale is the same as for Fig. 8.

OSD
8, 2377–2415, 2011

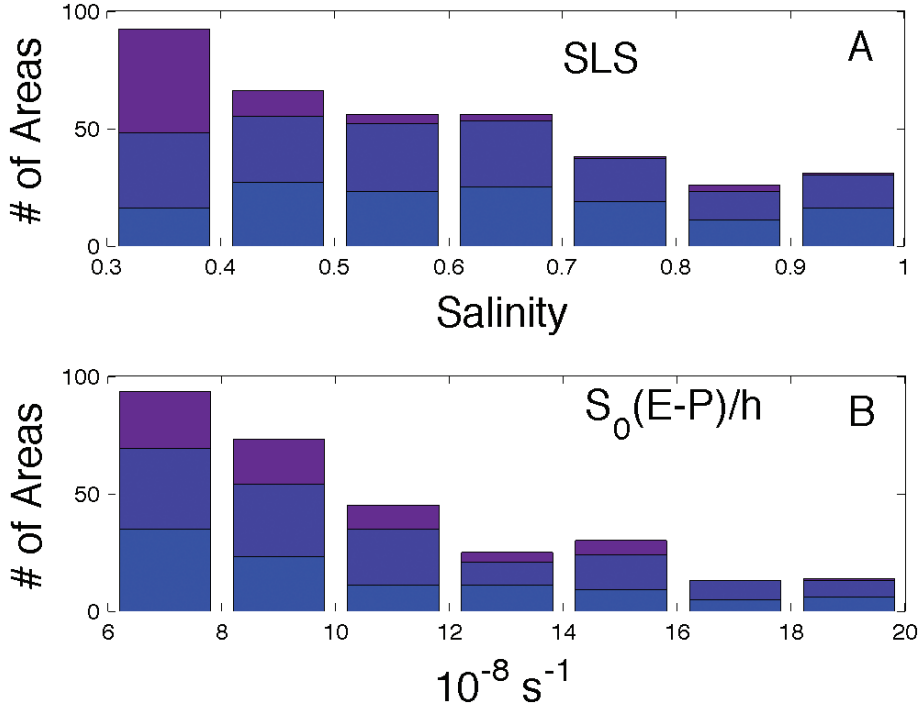

Fig. 10. As in Fig. 9, but for latitudes 0–30° N only, with different bins and *y*-axis limits emphasizing high amplitude areas.

OSD
8, 2377–2415, 2011

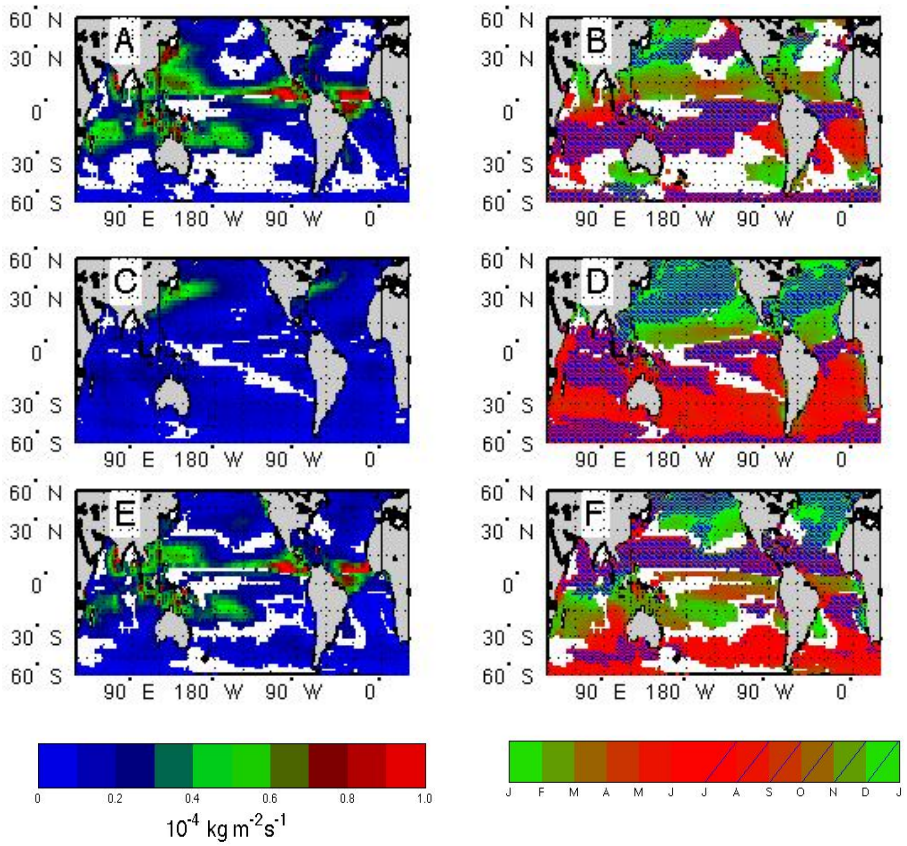

Fig. 11. Amplitude (left column) and phase (right column) of $E - P$ (top row), E (middle row) and P (bottom row). Amplitudes are in units of 10^{-4} kg m^{-2} s^{-1}. Ocean areas with no color had sufficient observations, but were found to have no significant seasonal cycle using a standard statistical test.

OSD
8, 2377–2415, 2011

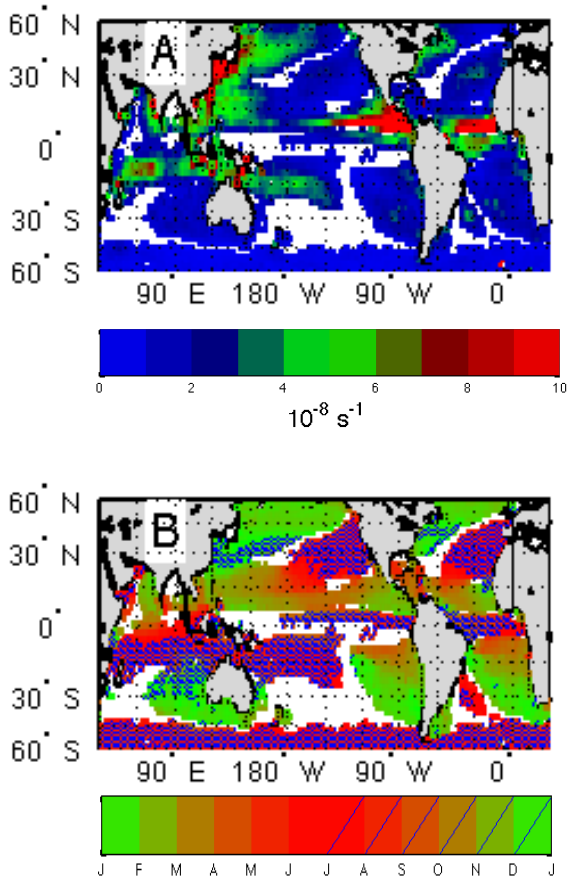

Fig. 12. Amplitude (top panel) and phase (bottom panel) of $S_0(E-P)/h$. Amplitudes are in units of $10^{-8}\,s^{-1}$. Phases are in units of months. Ocean areas with no color had sufficient observations, but were found to have no significant seasonal cycle using a standard statistical test.

OSD
8, 2377–2415, 2011

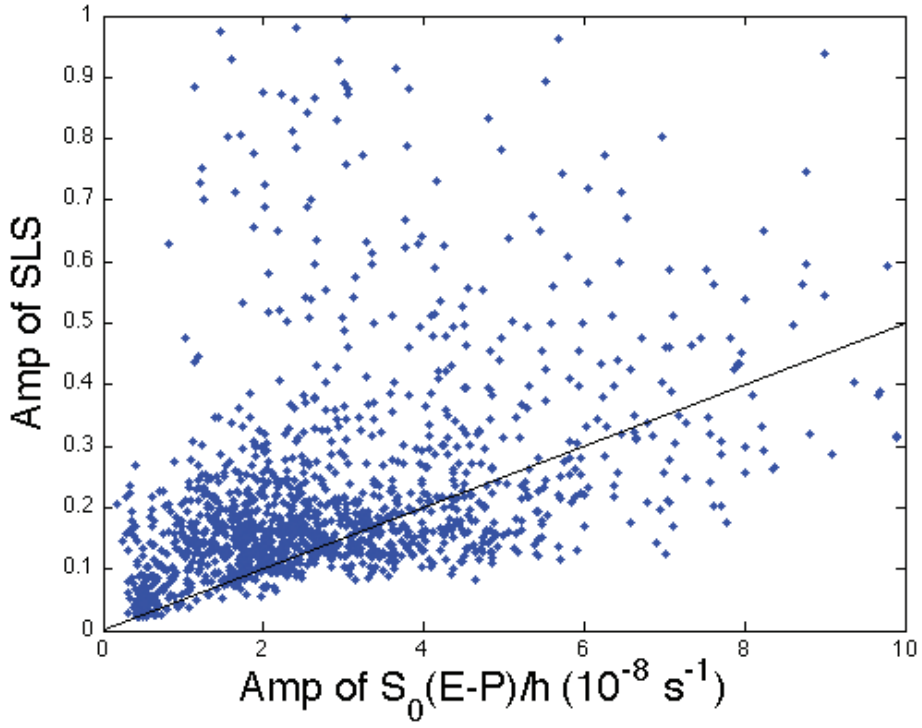

Fig. 13. Scatter plots comparing the amplitude of SLS (y-axis) and $S_0(E-P)/h$ (x-axis). Each dot represents a different 2.5° × 2.5° area. Light line is as discussed in the text.

OSD
8, 2377–2415, 2011

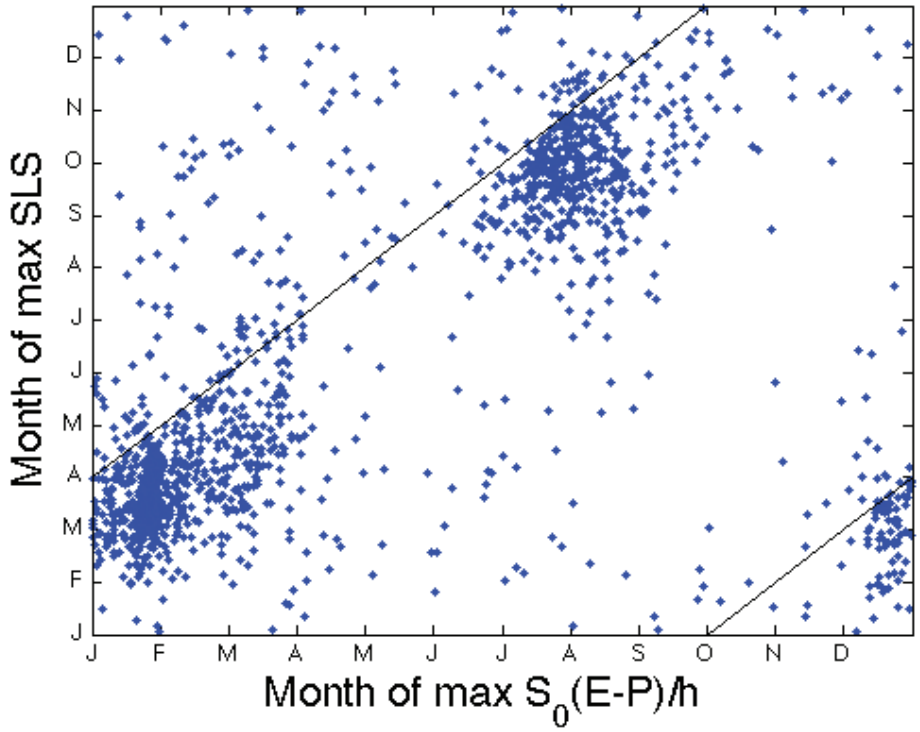

Fig. 14. Scatter plots comparing the phases of SLS (y-axis) and $S_0(E-P)/h$ (x-axis). Each dot represents a different $2.5^\circ \times 2.5^\circ$ area. The light line indicates a 3 month phase delay between $S_0(E-P)/h$ and SLS.

OSD
8, 2377–2415, 2011

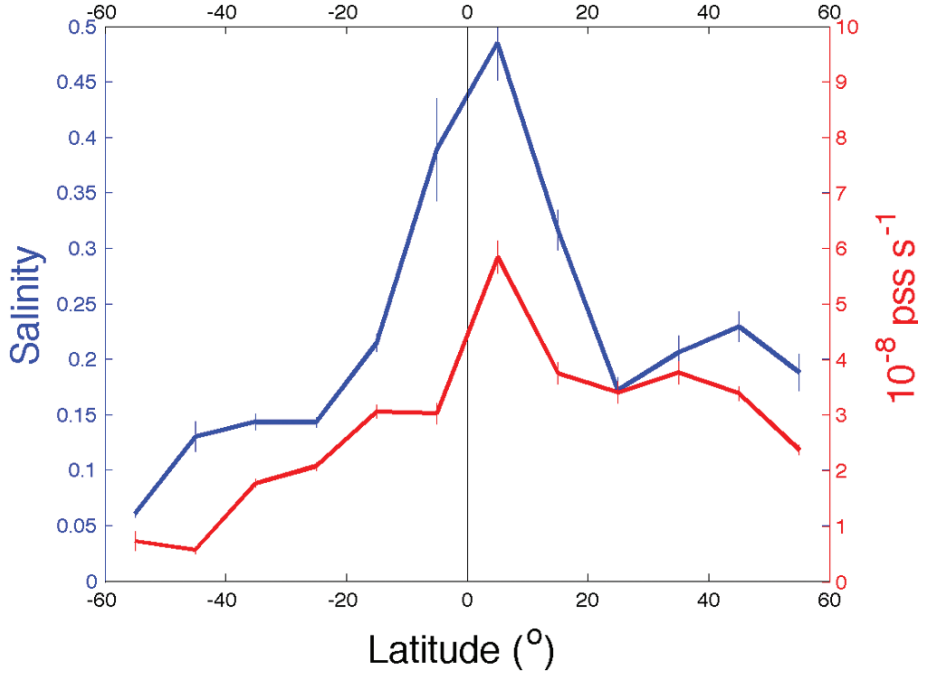

Fig. 15. Amplitude of SLS (blue line, left axis units) and $S_0(E-P)/h$ (red line, right axis units) averaged in 10° latitude bands. Error bars are standard error, i.e. standard deviation divided by the square root of the number of squares in each band.

OSD
8, 2377–2415, 2011

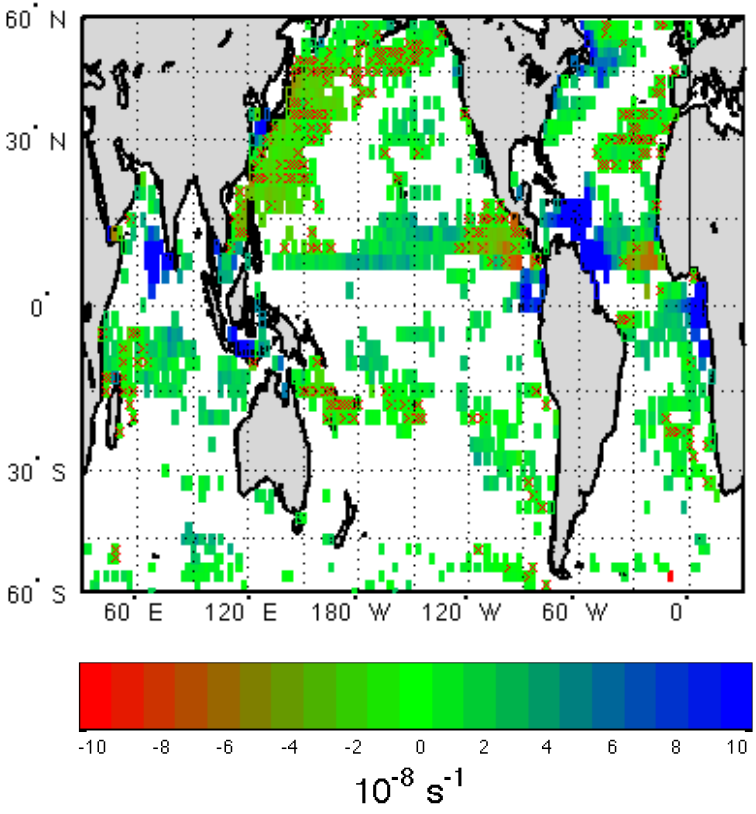

Fig. 16. Difference between amplitude of SLS and $S_0(E-P)/h$. A red "×" is overlaid on a 2.5° × 2.5° square when the two quantities are not significantly different from each other.

OSD
8, 2377–2415, 2011